ADVANCED MATERIALS
www.advmat.de

Functional, RF-Trilayer Sensors for Tooth-Mounted, Wireless Monitoring of the Oral Cavity and Food Consumption

*Peter Tseng, Bradley Napier, Logan Garbarini, David L. Kaplan, and Fiorenzo G. Omenetto**

Wearable devices have emerged as powerful tools for personalized healthcare in spite of some challenges that limit their widespread applicability as continuous monitors of physiological information. Here, a materials-based strategy to add utility to traditional dielectric sensors by developing a conformal radiofrequency (RF) construct composed of an active layer encapsulated between two reverse-facing split ring resonators is applied. These small (down to 2 mm × 2 mm) passive dielectric sensors possess enhanced sensitivity and can be further augmented by functionalization of this interlayer material. Demonstrator devices are shown where the interlayer is: (i) a porous silk film, and (ii) a modified PNIPAM hydrogel that swells with pH or temperature. In vivo use is demonstrated by adhesion of the device on tooth enamel to detect foods during human ingestion. Such sensors can be easily multiplexed and yield data-rich temporal information during the diffusion of analytes within the trilayer structure. This format could be extended to a suite of interlayer materials for sensing devices of added use and specificity.

Noninvasive medical devices are quickly emerging as powerful tools to provide data to assess individual health and wellness. In this context, conformal interfaces in the form of flexible devices and tattoos have emerged demonstrating measurement of physiological variables such as electricity, pressure, and/or analyte sensing[1–15] among others. In contrast to traditional, wearable devices that require mechanical fixation, such devices possess a low form factor and conform to surfaces, minimizing user impact while ensuring maximum proximity to the biological surface to be measured. Such sensors find use for monitoring of physiological parameters (such as glucose levels, hydration, heartrate, to name a few) and can be applied in constrained environments. For example, few accurate, low user burden methods exist for self-assessment of both intake and corresponding physiological responses to diet and nutrition.[16,17] In situ sensing of food consumption could potentially provide conclusive links between dietary intake and health. In order to directly access the oral cavity, several devices have been investigated, in particular mouthguard-based electrochemical sensors[12,13] or tooth tattoos.[4] The form factor and wiring requirements of electrochemical sensors prevent facile integration of these sensors into the mouth without a mechanical support (i.e., a mouthguard), while radiofrequency (RF)-sensing provides a more elegant solution, at the expense of dimensional challenges that can limit their in vivo application.

Conformal sensors typically rely on either dielectric or electrochemical sensing methodologies. Dielectric sensors probe an analyte (typically a biofluid) through its impedance spectrum, and can be configured for wireless sensing via radio waves.[18–24] Such sensors are easily fabricated in flexible, compact epidermal formats[3,4] and can utilize existing radiofrequency identification (RFID) infrastructure for data readout.[25] Typical drawbacks for these systems are the size imposed by the selected RF operational band, measurement inconsistency, and motion artifacts, and lower sensitivity to relevant biosignals such as sugars or pH. Electrochemical sensors rely on *redox* reactions occurring between an activated electrode surface and the analyte thus offering greater sensitivity than dielectric sensors at the expense of requiring a direct electrical connection to often bulky electrical measurement equipment that can significantly increase the device footprint even in mobile formats.[7,12,14] Furthermore, these devices are typically more expensive to fabricate (requiring immobilization of enzymes and biomolecules), possess a short operation window (several days due to inherent biofouling or enzyme degradation), and often require carbonaceous materials that have undetermined biocompatibility.[8,14,26]

Illustrated here is an approach to reduce the footprint of biosensing dielectric devices to the millimeter-scale thus extending the practical adoptability of such sensors. Specifically, the sensors are designed to fit onto a single human tooth to sample biofluids in the oral cavity and discriminate between consumed foods. A metamaterial-based approach[15,27–30] was adopted by using a broadside-coupled, split ring resonator (BC-SRR) geometry (composed of two stacked, reverse facing SRRs)[31] into a flexible format. BC-SRR geometries are favorable because of their combined small form factor and lower resonant frequency that make the devices practical for use with traditional RF instrumentation. In addition, the electric field is localized

Prof. P. Tseng,[+] B. Napier, L. Garbarini, Prof. D. L. Kaplan, Prof. F. G. Omenetto
Department of Biomedical Engineering
Tufts University
Medford, MA 02155, USA
E-mail: fiorenzo.omenetto@tufts.edu

The ORCID identification number(s) for the author(s) of this article can be found under https://doi.org/10.1002/adma.201703257.

[+]Present address: Department of EECS, UC Irvine, Irvine, CA 92697, USA

DOI: 10.1002/adma.201703257

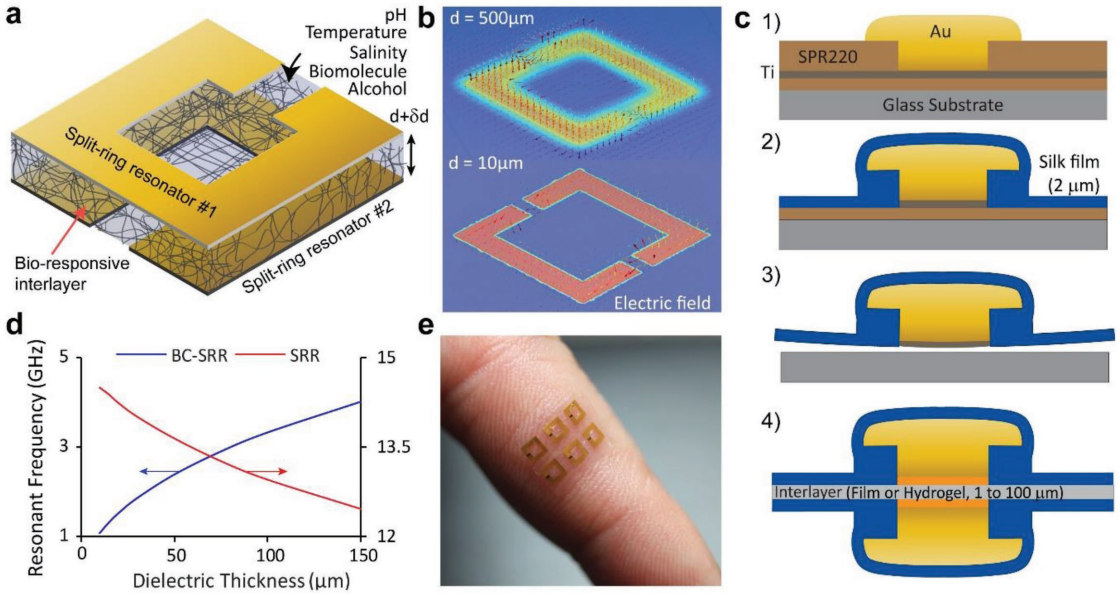

Figure 1. RF-trilayer sensors. a) Schematic of broad-side coupled split-ring resonators with an interlayer of silk film or responsive hydrogel. Interlayers swell and absorb surrounding solvent (changing thickness and dielectric constant) and result in a change in resonant frequency and amplitude of the sensor. b) Simulation (COMSOL Multiphysics) of the electric field of a 1 mm thick interlayer. Field lines focus within the structure and at the split-ring. Reducing interlayer thickness leads to increasing dominance of the interlayer capacitance as opposed to the split ring in the construct's resonant frequency. c) Abbreviated fabrication protocol. Split-ring resonators integrated into a silk film are used as the base for functional interlayers. d) Simulated resonant frequency of trilayer sensors in air with different thicknesses of interlayer (permittivity: 4). e) 2 mm element array applied to a human finger.

between the two resonators limiting the influence of the external environment on the device response. The sensor can conform to curved surfaces, such as the human tooth, and for this application the curvature of the sensor does not change during use. However, if applied to more dynamic surfaces, the effect of sensor bending on the resonant frequency during use (such as mechanical compression of the interlayer) should be taken into account and the materials and interfaces optimized for this purpose.

The sensing interlayer is sandwiched between individual split-ring resonators (**Figure 1**a). The device geometry makes the quality factor and resonant frequency of the antenna highly dependent on the interlayer, enhancing device performance in comparison to planar SRR-based dielectric sensors (Figure 1b). The construct enables: (i) detection of changes in interlayer thickness, (ii) engineerable delays in antenna response through controllable transport properties of solutes into the interlayer, and (iii) increased sensitivity due to the concentration of the E-field within the interlayer.

To confirm the usability of the device in biological environments, multiple devices were tested by immersion in saline solutions. The devices were found to maintain their format without visible delamination of the layers and a baseline operational frequency of $f_{\text{resonance}} \approx 400$ MHz was measured for a 3 mm × 3 mm device footprint. Devices down to 2 mm × 2 mm footprint were fabricated and showed a measurable resonant response.

To demonstrate the effectiveness of the interlayer as the functional element of the device, demonstrator trilayer constructs were assembled by including different materials between SRRs realized onto films of silk fibroin.[32–34] Silk is used as the outer layer of the device for its biocompatibility, its ability to controllably absorb and swell to different thicknesses in a variety of solvents (including water and ethanol), and its ability to be penetrated by biomolecules. The transport properties of silk films can also be regulated via the control of the protein conformation in film format.[35–38] Target demonstrations were explored by including interlayer materials that are responsive to analytes, temperature, or pH. Specifically, the materials encapsulated were a hygroscopic silk film, or hydrogel-based interlayers such as a silk gel or a responsive poly(N-isopropylacrylamide), PNIPAM-based hydrogel.[39–41]

Eigenfrequency simulations in COMSOL (RF module) were used to verify the resonant response of the SRRs and BC-SRRs with varying dielectric thickness. The dependence of the BC-SRR response to the thickness of the interlayer is confirmed by the size of the fringing fields that are of the same order of magnitude as the interlayer thickness (Figure 1b) as further illustrated by the relationship between the resonant frequency and the interlayer thickness (Figure 1d).

Constructs with silk film interlayers were evaluated in vitro in response to solvents with varying degrees of ionic strength, glucose concentration, and solvent concentration. Sensor performance while immersed in deionized (DI) water was found to be in agreement with the simulations. Devices with thinner interlayer films (≈1.2 μm) exhibited lower resonant frequencies (300–450 MHz), while thicker interlayer films (≈2.3 μm) exhibited higher resonant frequencies (525–650 MHz) in DI water. The sensor-to-sensor variation in resonant frequency (±100 MHz) and amplitude (−1 to −3 dB) is attributed to the manufacturing protocol of the devices, namely: (i) the different offset in the orientation/alignment of split-rings to each

other (any offset will increase the resonant frequency), and (ii) the uneven spin-coating of silk fibroin or uneven pressure distribution during trilayer sealing. These sensor-to-sensor variations affect the base resonant frequency which is measured in water prior to testing. Shifts from this base frequency are used to characterize the surrounding fluid. Due to these variations from fabrication, the sensors need to be calibrated in known solutions prior to performing measurements. It is expected that improvements in manufacturing would provide a consistent baseline and remove the need for this step.

To address simple examples of human food consumption, a single, thin-interlayer RF sensor was exposed to solutions including DI water, artificial saliva, 50% alcohol (ethanol), methanol, and high salinity saliva. Solution infiltration in the interlayers affects the response of the device by modulating its amplitude response and resonant frequency. Signals from the device were detected by using a RF network analyzer connected to a reading coil. Different analytes can be successfully discriminated as illustrated in **Figure 2**b. In the signals detected, in comparison to deionized water, artificial saliva possessed a lower amplitude (and slightly lower resonant frequency) due to its higher ionic strength, while alcohol led to an increase in the resonant frequency due to a lower net permittivity. Finally, higher-salinity artificial saliva led to a large reduction in amplitude (and a small reduction in resonant frequency). In general, it was easier to discriminate separate solutions in sensors with thinner interlayers than thicker ones (Figure S3, Supporting Information) likely because of the sharper resonance of thinner film devices and the associated higher sensitivity as a function of changes in interlayer thickness. Additional tests were performed by dissolving glucose in the solution under analysis. Increasing concentration of glucose leads to an increasing resonant frequency response of the sensor as its presence reduces the effective permittivity of solutions (Figure 2c). The corresponding temporal response of sensors to step-variations in glucose is shown in Figure S4 (Supporting Information). The trilayer displays sensitivities (in vitro) of around 0.6 MHz in 1 g L^{-1} of glucose (Figure 2c), well within the range required to detect sugar in drinks (e.g., fruit juice possesses up to 100 g L^{-1} sugar).

Due to the transient nature of solutions in the mouth, it is often desirable for a sensor to measure the average content of its surroundings to avoid signal fluctuations as saliva continuously mixes with food or drink. In the constructs presented here, the interlayer provides a short-term reservoir that averages solution concentrations over time. This time window

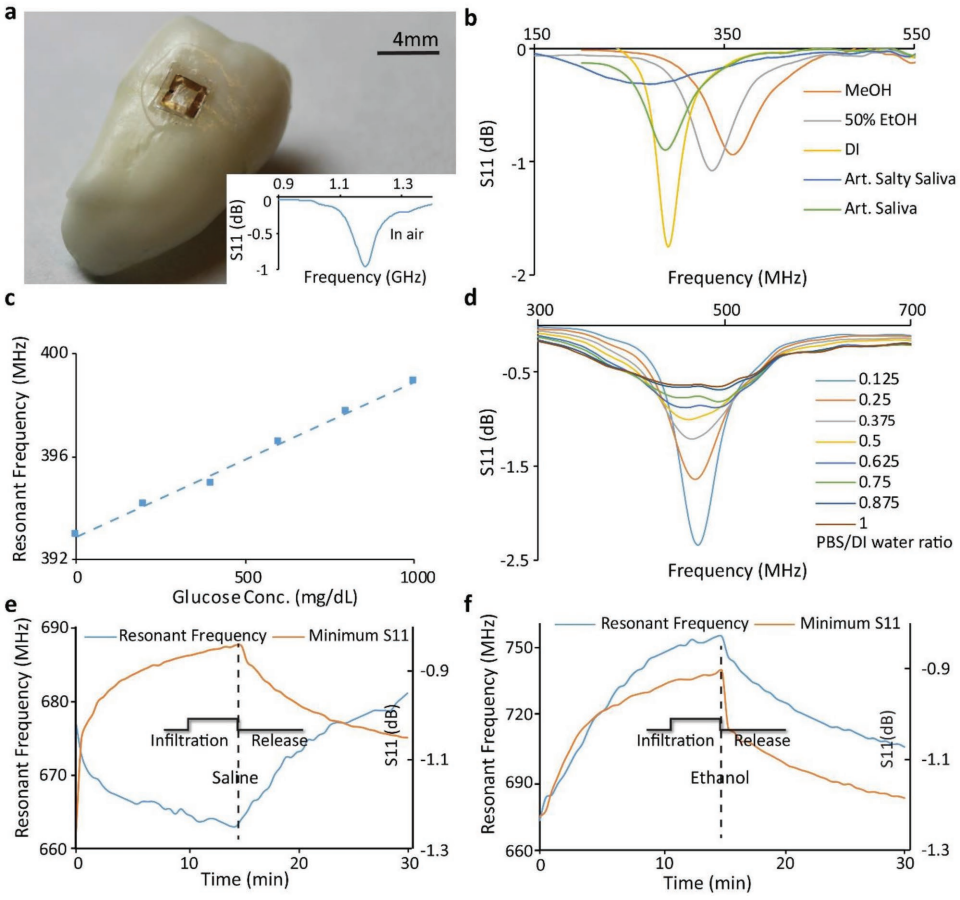

Figure 2. In vitro performance of biopolymer film-based sensors. a) 2 mm × 2 mm trilayer sensor conforming around a human tooth. Inset: Resonant response of the sensor when dry. b) Base response of a single thin interlayer (≈1.2 µm) sensor to various solvents and solutions. c) Changing resonant frequency of a thin interlayer sensor as a function of glucose concentration. d) Resonant response of a thin interlayer sensor as a function of salinity. e,f) Sensor temporal response of the same thick interlayer sensor (≈2.3 µm) to infiltration and release of high salinity and high alcohol concentrations.

can be controlled by the rate of solution penetration into the layer through the control of transport through the outer layers of the device. The response rates of thin (≈1.2 µm) and thick (≈2.3 µm) interlayer sensors from deionized water to 50% ethanol were tested (Figure S5, Supporting Information). Thicker films exhibited slightly faster response rates than thinner films, which is likely due to faster diffusion rates of solvents into the thicker interlayers. The general temporal response of trilayer sensors (≈2.3 µm thick) to infiltration and release of high-salt and high-alcohol solutions are shown in Figure 2e,f. Interestingly, we found infiltration and release rates to be negatively correlated. Exposure to high-salinity solutions rapidly reduced the signal amplitude, however the amplitude was slow to recover. The inverse was true for high-alcohol solutions: these exhibited lower penetration times yet faster reset times. These results are likely due to properties of the interlayer as silk possesses a relatively large net negative charge at physiological pH (to facilitate penetration of sodium ions), and is hygroscopic (with a slight preference for absorption of water over other solvents).

Interlayers composed of hydrogels were then examined by first using a soft (<10 kPa), ≈40 µm thick silk hydrogel[42,43] as the interlayer due to the adhesive properties of silk hydrogel to silk film and metals. Despite the differences in the respective thickness of hydrogel and film interlayers, sensors display similar resonant frequencies (≈400 MHz to 1 GHz). This is due to the higher effective permittivity of hydrogel interlayers due to water content. pH and temperature-sensitive interlayers can be achieved by using responsive PNIPAM hydrogels. These sensors experience a large frequency shift due to volume phase transitions of the hydrogel induced by temperature or pH that cause a thickness change of the layer. This response dominates over the decrease in permittivity that occurs due to this transition.[44] These gels exhibited poor adhesion properties when compared to the silk hydrogels, and thus required vapor pre-deposition of 3-methacryloxypropyltrimethoxysilane to facilitate covalent bonding between the titanium and hydrogel acrylate groups. Similar to previously described cases, we found variation in the base resonant frequency from sensor to sensor, this time mainly due to fluctuations in the gel thickness in the interlayer. The initial response of the PNIPAM loaded devices to varying temperatures is shown in **Figure 3**c. PNIPAM hydrogels collapse in size at around 35 °C, and this response was evident from temperature ramping (Figure 3c) and temperature relaxation (Figure S6, Supporting Information). Sensor response remained consistent across multiple

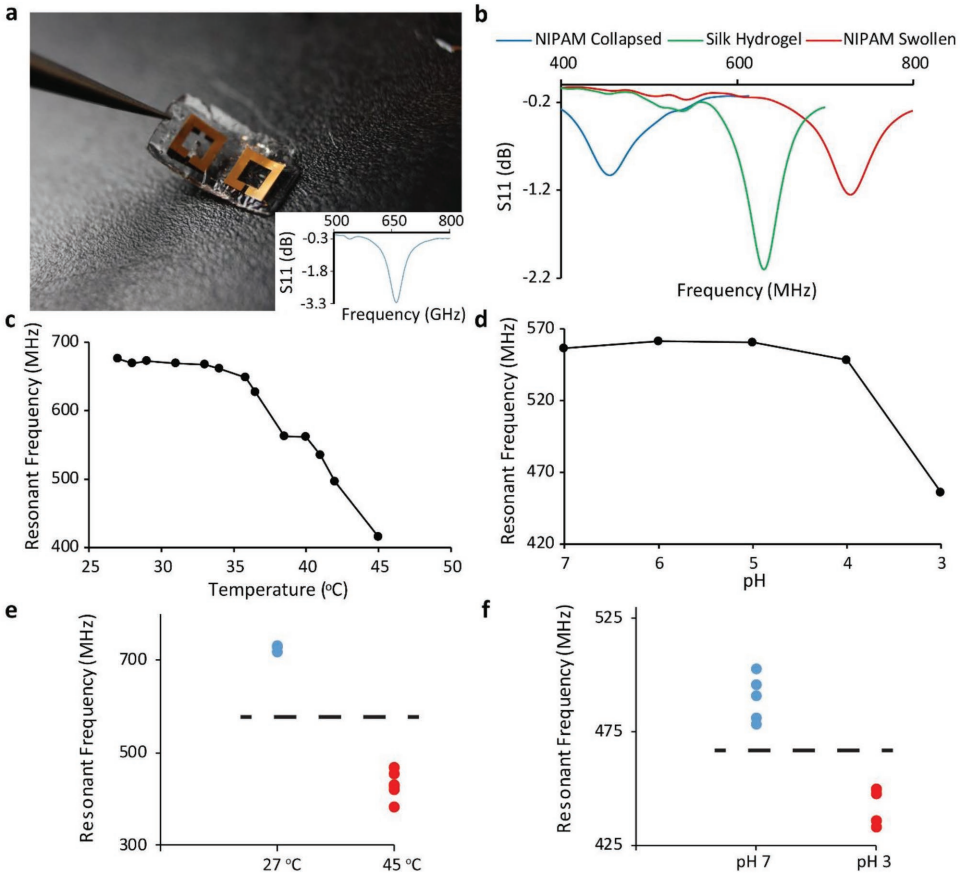

Figure 3. Development of responsive hydrogel-interlayer sensors. a) Image of silk hydrogel-interlayer structure. b) Comparison of spectral response from silk hydrogel and PNIPAM hydrogel (collapsed due to temperature and native swollen state). c) Initial shift in resonant frequency of a PNIPAM interlayer sensor as a function of temperature. d) Initial shift in resonant frequency of a PNIPAM interlayer sensor as a function of pH. e) Measured resonant frequency shifts of the sensor as a function of operational cycles when the temperature is cycled between 27 and 45 °C change in temperature. f) Measured resonant frequency shifts of the sensor as a function of repeated pH changes.

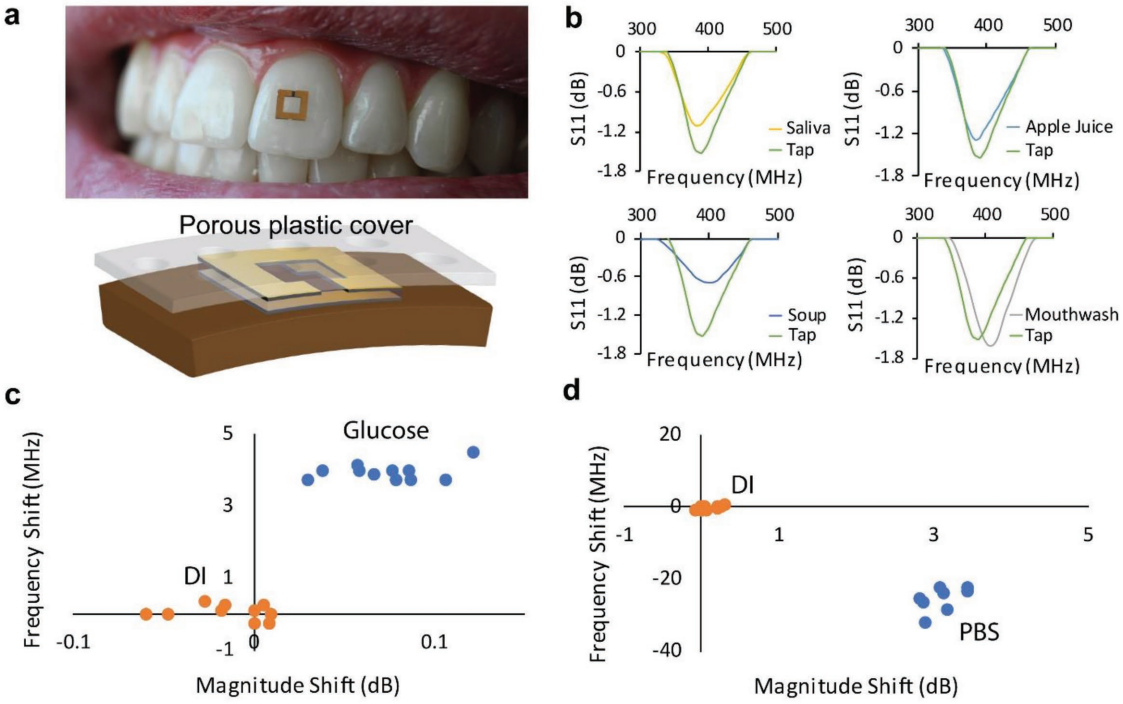

Figure 4. a) Trilayer sensor adhered to a human subject's tooth for in vivo monitoring of ingested fluids. b) Thin interlayer (≈1.2 µm) response on Subject 1 to various liquids. Changes to frequency and magnitude are seen in each case. c) Evaluation of benchtop response of sensor exposed to multiple repeated solution changes between DI and glucose (0.5 g dL^{-1}), and d) between DI and PBS. Magnitude and frequency shift of the resonant peak are plotted. The data show acceptable repeatability in the frequency response to both solutions over one week of data collection.

iterations with no noticeable change to the appearance of fabricated structures (Figure 3e). A second PNIPAM hydrogel-interlayer sensor was tested under changing pH (with constant ionic strength). Its resonant frequency dropped over 50 MHz upon exposure to a pH shift of 5 to 3 (Figure 3d). Similar to controlled changes in temperature, exposure of trilayer sensors to a changing pH leads to repeatable shifts in its resonant frequency (Figure 3f). For both temperature and pH, use of a responsive hydrogel enables discrimination between pH or temperature around a threshold determined by the properties of the hydrogel.

The functionality of silk-film trilayer sensors was evaluated for in vivo sensing of common liquid environments in the human mouth (**Figure 4**a). The study included measurements in dry-mouth conditions and following consumption of tap water, apple juice, alcohol, mouthwash, and soup. In total, four separate tests were performed on human subjects in accordance to approved institutional protocols. Three of the tests used thinner (≈1 µm) interlayers, while one trial tested an ≈2.3 µm thick interlayer. Figure 4b shows a representative trial result (data from other trials are shown in Figure S8, Supporting Information). The response of the trilayer devices was measured by using a mobile reader, composed of a portable vector network analyzer (VNA) attached to a tablet or cell phone (Figure S7, Supporting Information). The in vivo measurements exhibit similar trends to the in vitro measurements with shifts in resonant frequency and amplitude as a function of the different solvents, ionic strength, and presence of sugar. Consistent with previous measurements it was easier to discriminate liquids with structures that had thinner interlayers (data from thicker interlayer structures are shown in Figure S8b, Supporting Information). Preliminary in vivo studies on the responses/recovery time of sensors after exposure to soup (i.e., high salt), mouthwash, and drying are shown in Figure S8c–e (Supporting Information).

Finally, to assess the repeatability and stability of the sensor response to different, varying solutions, data from the sensors were taken over a period of a week with repeated changes between DI, PBS, and glucose (0.5 g L^{-1}) (Figure 4c,d). These data show that residual solute upon solution change is negligible with no appreciable shift in the baseline sensor response over time.

The broadside coupled multilayer antenna format combined with biopolymer-based permeable membranes and biologically active sensing layers provides an approach for a compact conformal platform for convenient sampling and sensing of analytes and sensing of foods and liquid consumption. By using interlayers composed of biopolymer films or responsive hydrogels, these constructs can be mounted directly onto human tooth enamel and become sensitized to a wide variety of fluid properties such as alcohol content, salinity, sugars, pH, temperature, with the opportunity of adding more specifically functionalized layers for targeted sensing. The few millimeter physical footprint makes these functional constructs convenient and adaptable to a variety of environments extending the applicability of RF sensors and allowing distributed, multiplexed sensing with the integration of additional responsive interlayers.

Experimental Section

Substrate Preparation: Fabrication of trilayer structures on flexible substrates was accomplished using a sacrificial layer technique.[45,46] Glass slides were cleaned in acetone, isopropanol, and oxygen plasma. A photoresist sacrificial layer was then spun and baked (spr-220, 3 µm) before e-beam deposition of Ti (30 nm)-Au (200 nm)-Ti (30 nm) as a seed layer. The photoresist was then coated and patterned to 7 µm (spr 220), the titanium overlayer was etched (1% HF), and gold was deposited via electroplating (Elevate Gold 7990, Technics). Gold was overplated to a thickness of 14 µm so as to create a mushroom structure. Seed layers were etched in titanium etchant (1% HF) followed by gold etchant (Transene), and then finished in titanium etchant. Silk fibroin (30 MB, prepared using established protocols) was dried onto substrates to form a thin 5 µm thick film and then water-annealed overnight in a high-humidity vacuum chamber. Water-soluble tape was then attached onto films to form a secondary substrate during release of silk film substrates of the carrier glass slide (with acetone).

To form silk film interlayer structures, silk fibroin (30 MB, 8%) was spun onto substrates to form a thin film. Separate films were then aligned and embossed together using a custom embossing setup (100 °C, 20 psi) to form a final, shelf stable structure composed of silk film-SRR trilayer flanked by water-soluble tape. Before studies, these structures were released from tape and pretreated over 24 h in deionized water.

To form hydrogel-interlayer structures, film-SRR structures were released from water-soluble tape with water, and rescaffolded onto plastic coverslips (Fischer). For silk hydrogel, silk hydrogel solution (15 µL, composed of 6% fibroin mixed with 10 U mL^{-1} of horseradish peroxidase and 0.01% hydrogen peroxide) was deposited above individual SRRs. The second half of the structure was then aligned and set above this first layer, and allowed to gel overnight. For PNIPAM hydrogel, NIPAM solution (composed of 10% NIPAM, 0.1% bis acrylamide, and 0.8% acrylic acid in DI) was combined with ammonium persulfate and TEMED to a final concentration of 0.8% APS and TEMED. 3 µL of solution was deposited between the SRR's. The solution was mixed at 0 °C to prevent premature gelation during mixing and allow rapid gelation when added to the room temp SRR's. Following gelation, the samples were placed in DI water overnight.

In Vitro Characterization: Resonant response of 3 mm × 3 mm antennas was characterized with a HP 8753E impedance analyzer using a small loop (3 mm) attached to the coaxial input. Interlayer structures were placed on a coverslip within a poly(dimethylsiloxane) (PDMS) stencil, and desired liquids were infiltrated within the stencil opening. A variety of liquids including deionized water, artificial saliva (Xialine 2 formulation), salty artificial saliva (200 mg L^{-1}), methanol, 50% ethanol, and various concentrations of salt and glucose in deionized water were tested.

In Vivo Characterization: For in vivo measurements, recently dried silk-fibroin interlayer sensors were attached to one side of double-sided tape (3M), and covered with a perforated thin plastic sheet. The opposite end of the double-sided tape was then affixed to the dried tooth of human subjects. Sensors were then allowed to rewet with subject saliva over 15 min before data were collected. For detection of base sensor response to different solvents, subjects were told to swish respective liquids (tap water, apple juice, cup noodle soup, or mouthwash) for ≈2 min before sensor response was collected. Resonant response of sensors was characterized with a miniVNA Tiny vector network analyzer. A small loop antenna (4 mm) with an attached 0.25 mm thick insulating plastic backing was used to gather data from the sensors. The plastic backing was gently placed on the resonator and the loop antenna was aligned to the sensor by eye before taking data.

Supporting Information

Supporting Information is available from the Wiley Online Library or from the author.

Acknowledgements

P.T. and B.N. contributed equally to this work. This research was sponsored by the U.S. Army Natick Soldier Research, Development and Engineering Center, and was accomplished under Cooperative Agreement No. W911QY-15-2-0001. The views and conclusions contained in this document are those of the authors and should not be interpreted as representing the official policies, either expressed or implied, of the U.S. Army Natick Soldier Research, Development and Engineering Center, or the U.S. Government. The U.S. Government is authorized to reproduce and distribute reprints for Government purposes notwithstanding any copyright notation hereon. P.T. acknowledges support for the NIH National Institute of Biomedical Imaging and Bioengineering under the NRSA fellowship F32EB021159. F.G.O. would like to acknowledge support from the Office of Naval Research (Grant No. N00014-13-1-0596) for this work. P. T., B.N., and F.O. contributed to initial concept and fabrication design. B.N. designed the test structures. P.T., B.N., and L.G. fabricated the structures. P.T. and B.N. designed the experiment. P.T., B.N., and L.G. performed both the in vitro and in vivo experiments. B.N. executed electromagnetic simulations in COMSOL. P.T., B.N., L.G., D.L.K. and F.O. wrote and commented on the manuscript. Experiments involving human subjects were performed with informed consent under protocol #12291 from the Tufts Health Sciences Institutional Review Board.

Conflict of Interest

The authors declare no conflict of interest.

Keywords

conformal sensing, epidermal electronics, flexible electronics, RF sensors

Received: June 11, 2017
Revised: January 14, 2018
Published online: March 23, 2018

[1] D.-H. Kim, N. Lu, R. Ma, Y.-S. Kim, R.-H. Kim, S. Wang, J. Wu, S. M. Won, H. Tao, A. Islam, K. J. Yu, T. Kim, R. Chowdhury, M. Ying, L. Xu, M. Li, H.-J. Chung, H. Keum, M. McCormick, P. Liu, Y.-W. Zhang, F. G. Omenetto, Y. Huang, T. Coleman, J. A. Rogers, *Science* **2011**, *333*, 838.
[2] S.-W. Hwang, H. Tao, D.-H. Kim, H. Cheng, J.-K. Song, E. Rill, M. A. Brenckle, B. Panilaitis, S. M. Won, Y.-S. Kim, Y. M. Song, K. J. Yu, A. Ameen, R. Li, Y. Su, M. Yang, D. L. Kaplan, M. R. Zakin, M. J. Slepian, Y. Huang, F. G. Omenetto, J. A. Rogers, *Science* **2012**, *337*, 1640.
[3] H. Tao, M. A. Brenckle, M. Yang, J. Zhang, M. Liu, S. M. Siebert, R. D. Averitt, M. S. Mannoor, M. C. McAlpine, J. A. Rogers, D. L. Kaplan, F. G. Omenetto, *Adv. Mater.* **2012**, *24*, 1067.
[4] M. S. Mannoor, H. Tao, J. D. Clayton, A. Sengupta, D. L. Kaplan, R. R. Naik, N. Verma, F. G. Omenetto, M. C. McAlpine, *Nat. Commun.* **2012**, *3*, 763.
[5] W. Jia, G. Valdés-Ramírez, A. J. Bandodkar, J. R. Windmiller, J. Wang, *Angew. Chem., Int. Ed.* **2013**, *52*, 7233.
[6] W. Jia, A. J. Bandodkar, G. Valdés-Ramírez, J. R. Windmiller, Z. Yang, J. Ramírez, G. Chan, J. Wang, *Anal. Chem.* **2013**, *85*, 6553.
[7] W. Gao, S. Emaminejad, H. Y. Y. Nyein, S. Challa, K. Chen, A. Peck, H. M. Fahad, H. Ota, H. Shiraki, D. Kiriya, D.-H. Lien, G. A. Brooks, R. W. Davis, A. Javey, *Nature* **2016**, *529*, 509.
[8] J. R. Windmiller, J. Wang, *Electroanalysis* **2013**, *25*, 29.
[9] T. Guinovart, A. J. Bandodkar, J. R. Windmiller, F. J. Andrade, J. Wang, *Analyst* **2013**, *138*, 7031.

[10] A. J. Bandodkar, D. Molinnus, O. Mirza, T. Guinovart, J. R. Windmiller, G. Valdés-Ramírez, F. J. Andrade, M. J. Schöning, J. Wang, *Biosens. Bioelectron.* **2014**, *54*, 603.
[11] X. Huang, Y. Liu, K. Chen, W.-J. Shin, C.-J. Lu, G.-W. Kong, D. Patnaik, S.-H. Lee, J. F. Cortes, J. A. Rogers, *Small* **2014**, *10*, 3083.
[12] J. Kim, G. Valdés-Ramírez, A. J. Bandodkar, W. Jia, A. G. Martinez, J. Ramírez, P. Mercier, J. Wang, *Analyst* **2014**, *139*, 1632.
[13] J. Kim, S. Imani, W. R. de Araujo, J. Warchall, G. Valdés-Ramírez, T. R. L. C. Paixão, P. P. Mercier, J. Wang, *Biosens. Bioelectron.* **2015**, *74*, 1061.
[14] H. Lee, T. K. Choi, Y. B. Lee, H. R. Cho, R. Ghaffari, L. Wang, H. J. Choi, T. D. Chung, N. Lu, T. Hyeon, S. H. Choi, D.-H. Kim, *Nat. Nanotechnol.* **2016**, *11*, 566.
[15] L. Y. Chen, B. C.-K. Tee, A. L. Chortos, G. Schwartz, V. Tse, D. J. Lipomi, H.-S. P. Wong, M. V. McConnell, Z. Bao, *Nat. Commun.* **2014**, *5*, 5028.
[16] T. M. Larsen, S.-M. Dalskov, M. van Baak, S. A. Jebb, A. Papadaki, A. F. H. Pfeiffer, J. A. Martinez, T. Handjieva-Darlenska, M. Kunešová, M. Pihlsgård, S. Stender, C. Holst, W. H. M. Saris, A. Astrup, *N. Engl. J. Med.* **2010**, *363*, 2102.
[17] F. M. Sacks, G. A. Bray, V. J. Carey, S. R. Smith, D. H. Ryan, S. D. Anton, K. McManus, C. M. Champagne, L. M. Bishop, N. Laranjo, M. S. Leboff, J. C. Rood, L. de Jonge, F. L. Greenway, C. M. Loria, E. Obarzanek, D. A. Williamson, *N. Engl. J. Med.* **2009**, *360*, 859.
[18] K. Asami, *J. Non-Cryst. Solids* **2002**, *305*, 268.
[19] G. J. Ciambrone, V. F. Liu, D. C. Lin, R. P. McGuinness, G. K. Leung, S. Pitchford, *J. Biomol. Screening* **2004**, *9*, 467.
[20] S. Gabriel, R. W. Lau, C. Gabriel, *Phys. Med. Biol.* **1996**, *41*, 2271.
[21] K. Heileman, J. Daoud, M. Tabrizian, *Biosens. Bioelectron.* **2013**, *49*, 348.
[22] T. L. Adamson, F. A. Eusebio, C. B. Cook, J. T. LaBelle, *Analyst* **2012**, *137*, 4179.
[23] R. K. Shervedani, A. H. Mehrjardi, N. Zamiri, *Bioelectrochemistry* **2006**, *69*, 201.
[24] M. S. Talary, F. Dewarrat, D. Huber, L. Falco-Jonasson, A. Caduff, in *13th Int. Conf. Electrical Bioimpedance 8th Conf. Electrical Impedance Tomography* (Eds: H. Scharfetter, R. Merwa), Springer,Berlin **2007**, pp. 636–639.
[25] J. M. Azzarelli, K. A. Mirica, J. B. Ravnsbæk, T. M. Swager, *Proc. Natl. Acad. Sci. USA* **2014**, *111*, 18162.
[26] D. Du, P. Li, J. Ouyang, *J. Mater. Chem. C* **2016**, *4*, 3224.
[27] H.-J. Lee, J.-G. Yook, *Appl. Phys. Lett.* **2008**, *92*, 254103.
[28] H.-J. Lee, H.-S. Lee, K.-H. Yoo, J.-G. Yook, *J. Appl. Phys.* **2010**, *108*, 14908.
[29] H.-J. Lee, J.-H. Lee, H.-S. Moon, I.-S. Jang, J.-S. Choi, J.-G. Yook, H.-I. Jung, *Sens. Actuators, B* **2012**, *169*, 26.
[30] S. Roy Choudhury, V. Rawat, A. H. Jalal, S. N. Kale, S. Bhansali, *Biosens. Bioelectron.* **2016**, *86*, 595.
[31] E. Ekmekci, A. C. Strikwerda, K. Fan, G. Keiser, X. Zhang, G. Turhan-Sayan, R. D. Averitt, *Phys. Rev. B* **2011**, *83*, 193103.
[32] M. A. Brenckle, H. Tao, S. Kim, M. Paquette, D. L. Kaplan, F. G. Omenetto, *Adv. Mater.* **2013**, *25*, 2409.
[33] X. Chen, Z. Shao, D. P. Knight, F. Vollrath, *Proteins* **2007**, *68*, 223.
[34] D. N. Rockwood, R. C. Preda, T. Yücel, X. Wang, M. L. Lovett, D. L. Kaplan, *Nat. Protoc.* **2011**, *6*, 1612.
[35] B. Marelli, M. A. Brenckle, D. L. Kaplan, F. G. Omenetto, *Sci. Rep.* **2016**, *6*, 25263.
[36] M. A. Brenckle, H. Cheng, S. Hwang, H. Tao, M. Paquette, D. L. Kaplan, J. A. Rogers, Y. Huang, F. G. Omenetto, *ACS Appl. Mater. Interfaces* **2015**, *7*, 19870.
[37] D. J. Hines, D. L. Kaplan, *Biomacromolecules* **2011**, *12*, 804.
[38] E. M. Pritchard, D. L. Kaplan, *Expert Opin. Drug Delivery* **2011**, *8*, 797.
[39] T. Hoare, R. Pelton, *Macromolecules* **2004**, *37*, 2544.
[40] J. Zhang, L.-Y. Chu, Y.-K. Li, Y. M. Lee, *Polymer* **2007**, *48*, 1718.
[41] X. Gao, Y. Cao, X. Song, Z. Zhang, C. Xiao, C. He, X. Chen, *J. Mater. Chem. B* **2013**, *1*, 5578.
[42] B. P. Partlow, C. W. Hanna, J. Rnjak-Kovacina, J. E. Moreau, M. B. Applegate, K. A. Burke, B. Marelli, A. N. Mitropoulos, F. G. Omenetto, D. L. Kaplan, *Adv. Funct. Mater.* **2014**, *24*, 4615.
[43] P. Tseng, B. Napier, S. Zhao, A. N. Mitropoulos, M. B. Applegate, B. Marelli, D. L. Kaplan, F. G. Omenetto, *Nat. Nanotechnol.* **2017**, *12*, 474.
[44] M. Yang, C. Liu, Y. Lian, K. Zhao, D. Zhu, J. Zhou, *Soft Matter* **2017**, *13*, 2663.
[45] P. Tseng, I. Pushkarsky, D. Di Carlo, *PLoS One* **2014**, *9*, e106091.
[46] P. Tseng, J. Lin, K. Owsley, J. Kong, A. Kunze, C. Murray, D. Di Carlo, *Adv. Mater.* **2015**, *27*, 1083.

